

# Artificial Neural Network Controller for Reducing the Total Harmonic Distortion (THD) in HVDC

Dr. Ali Nathem Hamoodi, Rasha Abdul-nafaa Mohammed

<sup>1</sup>Lect., Dept. of Technical Power Eng., Technical College-Mosul  
<sup>2</sup>Asist. Lect., Dept. of Technical Power Eng, Technical College-Mosul

**Abstract**— A neural network based space vector modulation (SVM) of voltage source inverter is proposed. The voltage source converter (VSC) is highly used in high voltage direct current (HVDC) transmission so that a detailed analysis and transmission of this system is carried out. In addition, a non-linear neural network controller is proposed to control the space vector pulse width modulation (SVPWM) to reduce the total harmonic distortion (THD) of the converter (inverter) output voltage. The inverter output current is analyzed with two switching frequency 1050Hz and 1450Hz with and without proposed ANN controller. The results show a THD enhancement about 0.74 % for 1050Hz and 0.68 % for 1450Hz.

**Keywords**— HVDC, VSC, THD , SVPWM, ANN.

## I. INTRODUCTION

An electronic converter is required to convert DC to AC energy . VSC is used to interconnect generation system with AC network. Now VSC is one of the best converter because it has modern power semiconductor advantages as Turn-off (GTO) and (IGBT) [1-2].

The flow control of active and reactive power flow is become more flexible today because of VSC-HVDC technology [3-6].

The basic VSC model is shown in figure.(1).

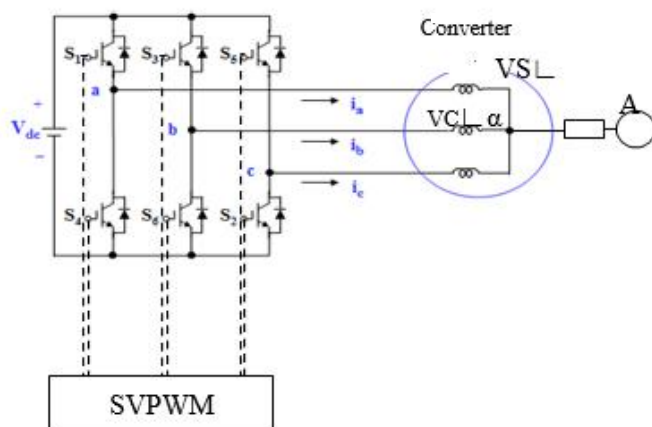


Fig.1: Model of six-pulse VSC-HVDC system.

This paper describes neural network controller based on SVPWM implementation of a 12-pulse voltage-fed inverter. In the beginning, (SVPWM) for a 12-pulse inverter is reviewed briefly. The general expressions of time segments of inverter voltage vector for all the regions have been derived.

A basic 12-pulse VSC-HVDC system is comprised of two 6-pulse IGBT converter station built with VSC topologies as shown in figure.(2)

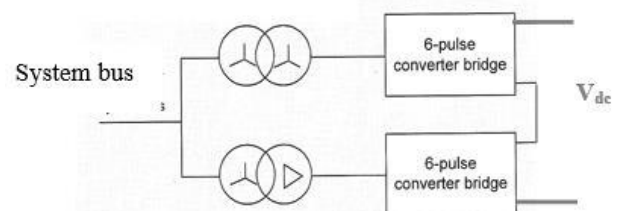


Fig.2: Series connection on DC sides

(SVPWM) has modern technology for voltage fed converter. It consider more improved as compared with PWM [7].

## II. SVPWM TECHNIQUE.

SVPWM considered as best method for digital implementations where, switching frequency(2/3) [9,10]. The 6-switch three-phase voltage source inverter is shown in figure.3

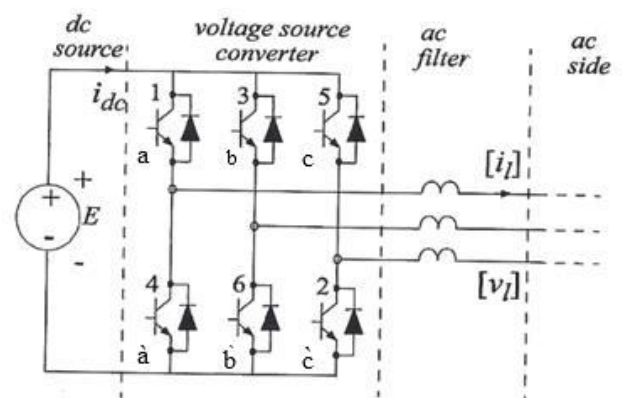


Fig.3: Six-switch three-phase voltage source inverter.

### III. SWITCHING SEQUENCES.

In 3Φ inverter, the outputted voltage vectors with six sectors as illustrated in figure.4. [11].

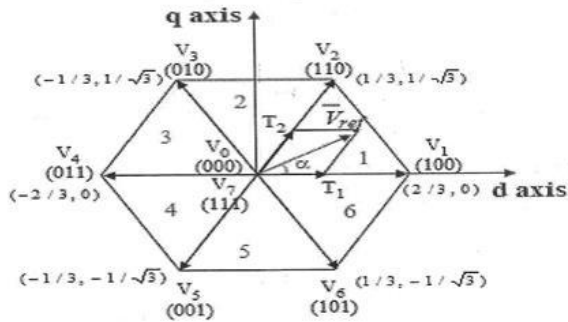


Fig.4: Basic switching vectors and sectors.

Where,  
 (2Tz): sampling time.  
 V\*:command vector.  
 A: angle in each sector.

The eight switching sequences is shown in figure.5.

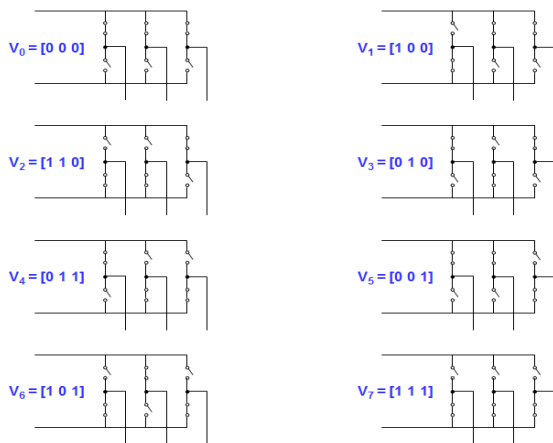


Fig.5: Switching sequences.

The eight combination, voltage vectors, switching sequences, phase voltages and output line to line voltages is shown in Table.1.

Table.1: Voltage vectors, switching sequences, phase voltages and line-to-line voltages.

Voltage Vectors	Switching Vectors			Line to neutral voltage			Line to line voltage		
	a	b	c	V <sub>an</sub>	V <sub>bn</sub>	V <sub>cn</sub>	V <sub>ab</sub>	V <sub>bc</sub>	V <sub>ca</sub>
V <sub>0</sub>	0	0	0	0	0	0	0	0	0
V <sub>1</sub>	1	0	0	2/3	-1/3	-1/3	1	0	-1
V <sub>2</sub>	1	1	0	1/3	1/3	-2/3	0	1	-1
V <sub>3</sub>	0	1	0	-1/3	2/3	-1/3	-1	1	0
V <sub>4</sub>	0	1	1	-2/3	1/3	1/3	-1	0	1
V <sub>5</sub>	0	0	1	-1/3	-1/3	2/3	0	-1	1
V <sub>6</sub>	1	0	1	1/3	-2/3	1/3	1	-1	0
V <sub>7</sub>	1	1	1	0	0	0	0	0	0

(Note that the respective voltage should be multiplied by V<sub>dc</sub> )

### IV. REALIZATION OF SVPWM.

In order to realize the SVPWM , three steps must be investigated .

- Determining the voltages.
- Determining time durations.
- Determining the switching time.

The voltages in a, b, c, frame is transformed to space vector voltage in d-q frame shown in figure.6

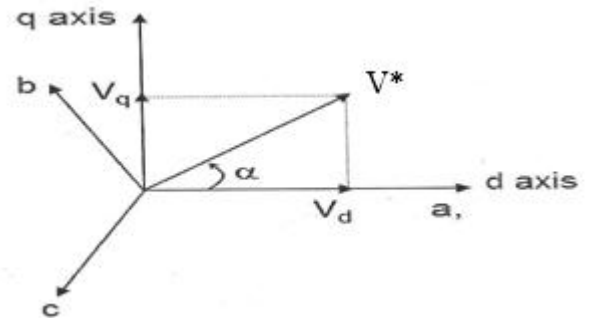


Fig. 6: Space vector in (d,q) frame.

V<sub>d</sub> and V<sub>q</sub> can be represented as:

$$\therefore \begin{bmatrix} V_d \\ V_q \end{bmatrix} = \frac{2}{3} \begin{bmatrix} 1 & -\frac{1}{2} & -\frac{1}{2} \\ 0 & \frac{\sqrt{3}}{2} & -\frac{\sqrt{3}}{2} \end{bmatrix} \begin{bmatrix} V_{an} \\ V_{bn} \\ V_{cn} \end{bmatrix} \dots\dots\dots(1)$$

$$|\bar{V}^*| = \sqrt{V_d^2 + V_q^2} \dots\dots\dots(2)$$

$$\alpha = \tan^{-1} \left( \frac{V_q}{V_d} \right) \dots\dots\dots(3)$$

$$\omega_s t = 2\pi f_s t$$

where,

f<sub>s</sub> = switching frequency

α = Vector angle

V<sub>d</sub> = horizontal component.

V<sub>q</sub> = vertical component.

$\bar{V}^*$  = the vector of V<sub>ref</sub>.

- Determining time duration.

The terns router combination is depicted in figure.7.

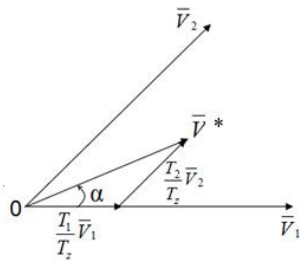


Fig.7: Reference vector combination.

The switching time duration at any sector is determined by the following equations:[12].

$$\begin{aligned} \therefore T_1 &= \frac{\sqrt{3} \cdot T_z \cdot |\bar{V}^*|}{V_{dc}} \left( \sin\left(\frac{\pi}{3} - \alpha + \frac{n-1}{3}\pi\right) \right) \\ &= \frac{\sqrt{3} \cdot T_z \cdot |\bar{V}^*|}{V_{dc}} \left( \sin\frac{n}{3}\pi - \alpha \right) \\ &= \frac{\sqrt{3} \cdot T_z \cdot |\bar{V}^*|}{V_{dc}} \left( \sin\frac{n}{3}\pi \cos\alpha - \cos\frac{n}{3}\pi \sin\alpha \right) \dots\dots\dots(4) \end{aligned}$$

$$\begin{aligned} \therefore T_2 &= \frac{\sqrt{3} \cdot T_z \cdot |\bar{V}^*|}{V_{dc}} \left( \sin\left(\alpha - \frac{n-1}{3}\pi\right) \right) \\ &= \frac{\sqrt{3} \cdot T_z \cdot |\bar{V}^*|}{V_{dc}} \left( -\cos\alpha \cdot \sin\frac{n-1}{3}\pi + \sin\alpha \cdot \cos\frac{n-1}{3}\pi \right) \end{aligned} \dots\dots\dots(5)$$

$$\therefore T_0 = T_z - (T_1 + T_2), \begin{cases} \text{(where, } n=1 \text{ through } 6) \\ \text{(that is, Sector 1 to 6)} \\ 0 \leq \theta \leq 60^\circ \end{cases} \dots\dots\dots(6)$$

Where,

$T_1, T_2$  and  $T_0$ : is the time duration for each sector.

$T_z$ : is the sampling time ( inverse of the switching frequency ( $f_s$ )).

c-Determining the switching time of each transistor ( $S_1$  to  $S_6$ ). The switching times of the upper and lower transistors for each sector is shown in figure.8

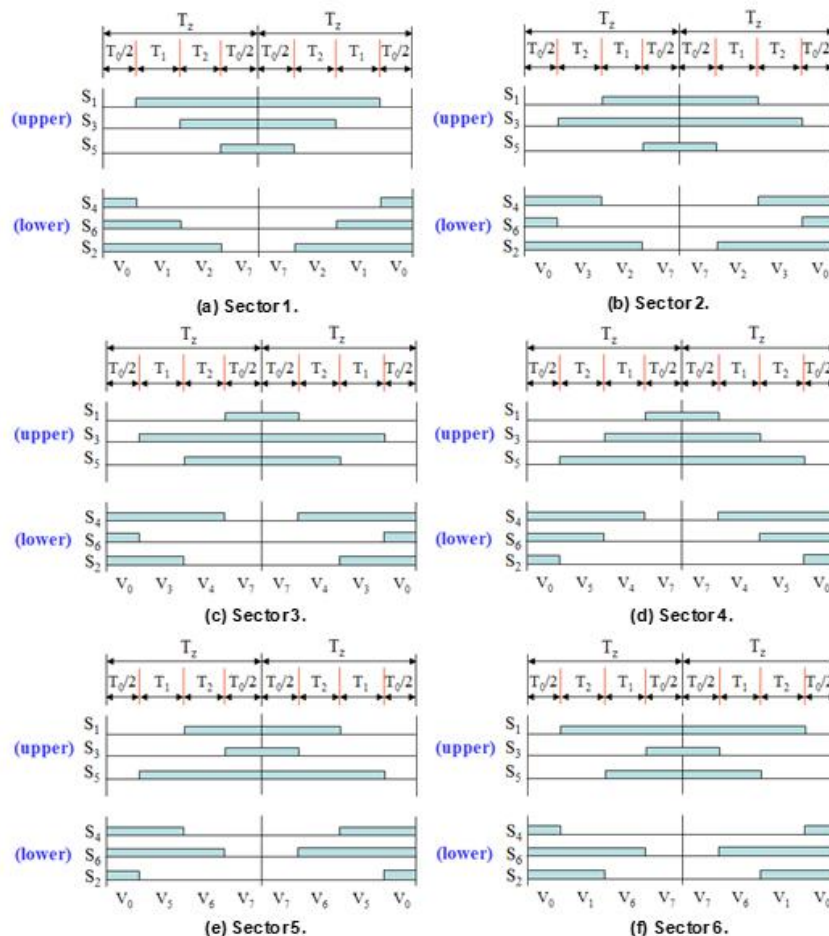


Fig. 8: PWM patterns at each sector.

V. SIMULATION WITHOUT ANN IMPLICATION VSI-HVDC BASED SVPWM.

Figure.9 presents Matlab/Simulinkmodel of a 12-pluse VSI-HVDC based on SVPWM.

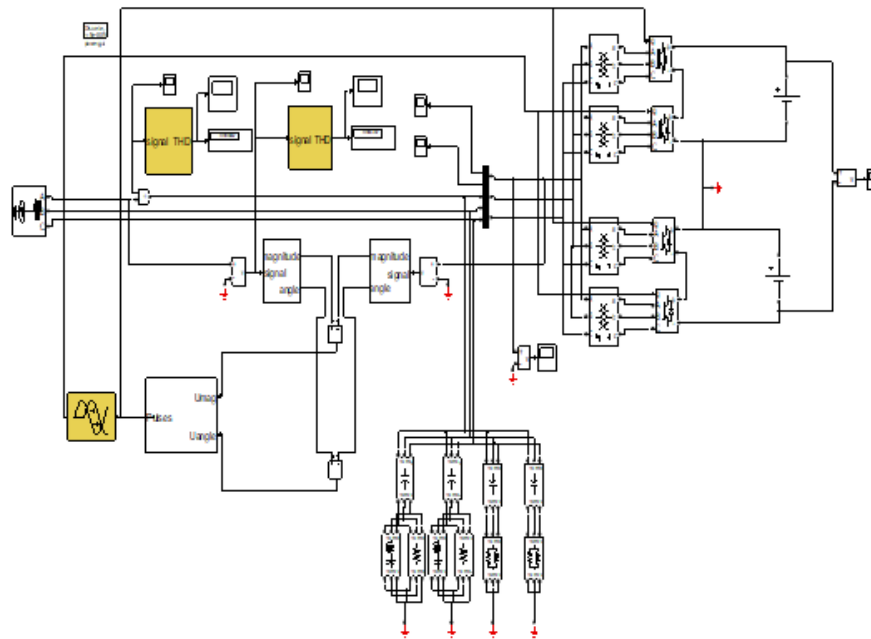


Fig.9: MATLAB/SIMULINK model of a VSI-HVDC on SVPWM.

The THD ratio of the line current for switching frequencies 1050Hz and 1450Hz is shown in figure. 10.

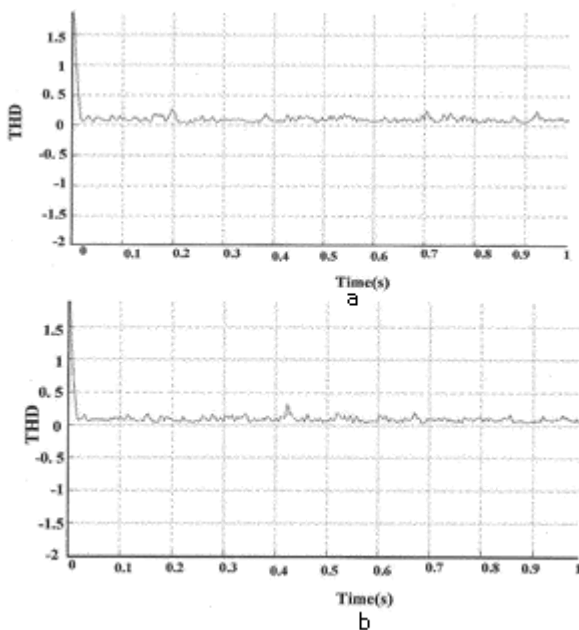


Fig.10: THD ratio of line current in time domain.  
 (a) at switching frequency (1050Hz).  
 (b) at switching frequency (1450Hz).

The THD ratio of the line to line voltage at 1050Hz and 1450Hz switching frequency is shown in figure.11.

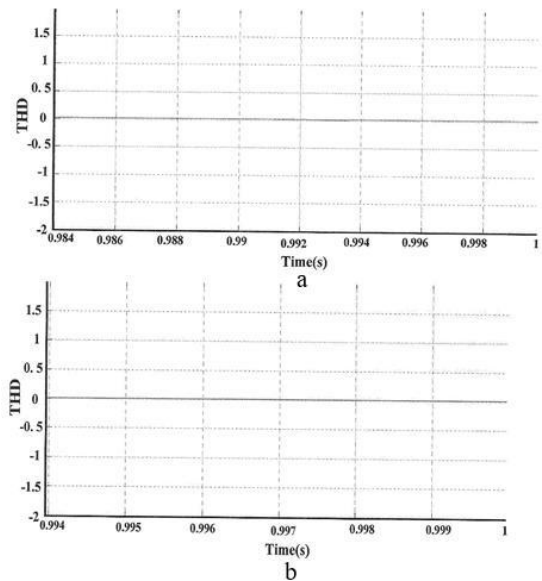


Fig.11: THD ratio of line to line voltage in time domain.  
 (a) at switching frequency (1050Hz).  
 (b) at switching frequency (1450Hz).

The THD ratio of the line current and line-line voltage shown in Table.2 are obtained directly by computer from figures 10 & 11.

Table.2: THD values for line current and line to line voltage

Switching frequency(Hz)	Line current THD value(%)	Line-line Voltage THD value(%)
1050	17%	2.088%
1450	8.625%	1.323%

**VI. TRAINING METHOD**

In this paper, back propagation Levenberg- marquard (LM) algorithm is used for training converter because this method has many advantages and gives high response .Leverberg-marquard (LM) algorithm is used.

**VII. ANN-BASED SVPW IMPLICATION.**

A feed forward ANN mapping and its timing calculation, the turn-on time  $T_{-ON}$  given as:[13].

$$T_{-ON} = \begin{cases} \frac{T_z}{2} + D |V^*| \begin{bmatrix} -\left(\sin \frac{n}{3}\pi \cos \theta - \cos \frac{n}{3}\sin \alpha\right) \\ -\left(-\cos \theta \sin \frac{n-1}{3}\pi + \sin \theta \cos \frac{n-1}{3}\pi\right) \end{bmatrix} \text{Sector} \\ \frac{T_z}{2} + D |V^*| \begin{bmatrix} -\left(\sin \frac{n}{3}\pi \cos \theta - \cos \frac{n}{3}\sin \theta\right) \\ +\left(-\cos \theta \sin \frac{n-1}{3}\pi + \sin \theta \cos \frac{n-1}{3}\pi\right) \end{bmatrix} \text{Sector} \\ \frac{T_z}{2} + D |V^*| \begin{bmatrix} +\left(\sin \frac{n}{3}\pi \cos \theta - \cos \frac{n}{3}\sin \theta\right) \\ +\left(-\cos \theta \sin \frac{n-1}{3}\pi + \sin \theta \cos \frac{n-1}{3}\pi\right) \end{bmatrix} \text{Sector} \\ \frac{T_z}{2} - D |V^*| \begin{bmatrix} +\left(\sin \frac{n}{3}\pi \cos \theta - \cos \frac{n}{3}\sin \theta\right) \\ -\left(-\cos \theta \sin \frac{n-1}{3}\pi + \sin \theta \cos \frac{n-1}{3}\pi\right) \end{bmatrix} \text{Sector} \end{cases}$$

where,

$$D = \sqrt{3} \times V_{ref} / V_{dc}$$

Turn-off time is depicted as:

$$T_{-OFF} = 2T_z - T_{A-on} \dots \dots \dots (8)$$

In general, from equation (12) can be written as:

$$T_{-ON} = \frac{T_z}{2} + f(V^*) \cdot g(\alpha) \dots \dots \dots (9)$$

where ,

$f(V^*)$  is the voltage amplitude scale factor.

And

$$g(\alpha) = \begin{cases} D \begin{bmatrix} -\left(\sin \frac{n}{3}\pi \cos \alpha - \cos \frac{n}{3}\sin \alpha\right) \\ -\left(-\cos \alpha \sin \frac{n-1}{3}\pi + \sin \alpha \cos \frac{n-1}{3}\pi\right) \end{bmatrix} \text{Sector} = 1,6 \\ D \begin{bmatrix} -\left(\sin \frac{n}{3}\pi \cos \alpha - \cos \frac{n}{3}\sin \alpha\right) \\ +\left(-\cos \alpha \sin \frac{n-1}{3}\pi + \sin \alpha \cos \frac{n-1}{3}\pi\right) \end{bmatrix} \text{Sector} = 2 \\ D \begin{bmatrix} +\left(\sin \frac{n}{3}\pi \cos \alpha - \cos \frac{n}{3}\sin \alpha\right) \\ +\left(-\cos \alpha \sin \frac{n-1}{3}\pi + \sin \alpha \cos \frac{n-1}{3}\pi\right) \end{bmatrix} \text{Sector} = 3,4 \\ D \begin{bmatrix} +\left(\sin \frac{n}{3}\pi \cos \alpha - \cos \frac{n}{3}\sin \alpha\right) \\ -\left(-\cos \alpha \sin \frac{n-1}{3}\pi + \sin \alpha \cos \frac{n-1}{3}\pi\right) \end{bmatrix} \text{Sector} = 5 \end{cases} \dots \dots \dots (10)$$

$g(\alpha)$ : T-on pulse width.

In the under modulation region,  $f(V^*) = V^*$  as depicted in figure. 12.

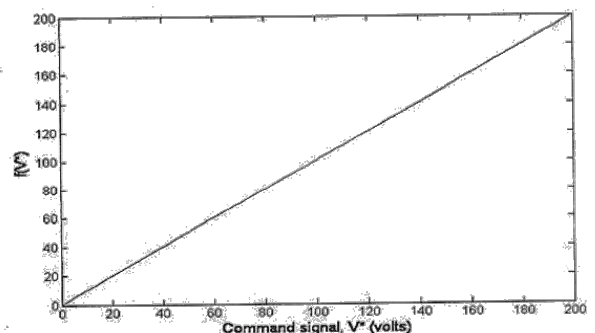


Fig.12:  $f(V^*)$ - $V^*$  relation in under modulation region  
 The pulse generated by ANN for sector one , $V^* = 360KV$  and  $\theta = 40^\circ$  as taken from the inverter side, is shown in figure.13.



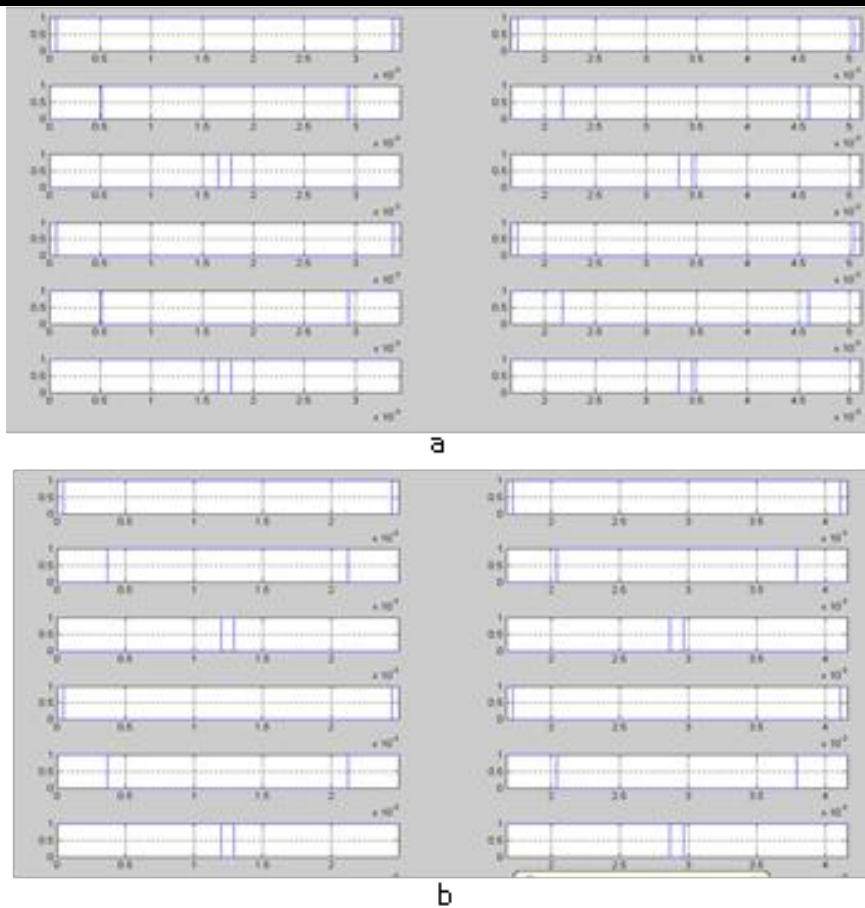


Fig.13: PWM using ANN.  
 (a) at switching frequency (1050Hz).  
 (b) At switching frequency (1450Hz).

### VIII. SUGGESTED TOPOLOGY OF ANN BASED CONTROLLER

The ANN suggested topology has two inputs (two neurons) in the input layer, one hidden layer (N- neurons) and three outputs (three neurons) in the output layer. The input layer simply acts as a fan-out input to the hidden layer where two neurons are used and the output layer has three neurons with a sigmoidal activation function and (N) inputs (N1 from the hidden layer and one constant bias).

The input layer of the proposed ANN controller shown in figure (14) has two input variables, the first is the  $V_{ref\text{vector}} \left| \bar{V}^* \right|$  and the second vector angle  $\alpha$ . While, the output layer has two variables concerned with the on and off durations of the switching pulses. The error which represented by the target minus the actual the delta rule [9].

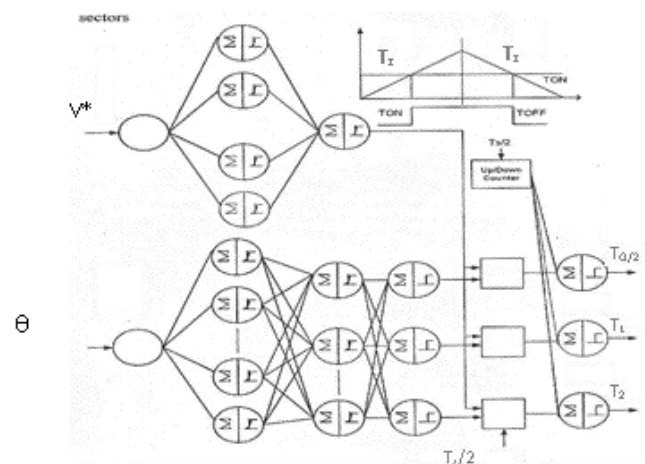


Fig. 14: ANN topology for PWM pulse generating using SVPWM.

The THD ratio of line current and line to line voltage by using NN based SVPWM is shown in table .3.

Table.3: THD ratio of line current and line to line voltage by NN based SVPWM.

Switching frequency(Hz)	Line current THD value(%)	Line -line Voltage THD value(%)
1050	4.308 %	0.4535 %
1450	2.744 %	0.4535 %

Figure. 15 represents the circuit diagram of VSI-HVDC using ANN based SVPWM.

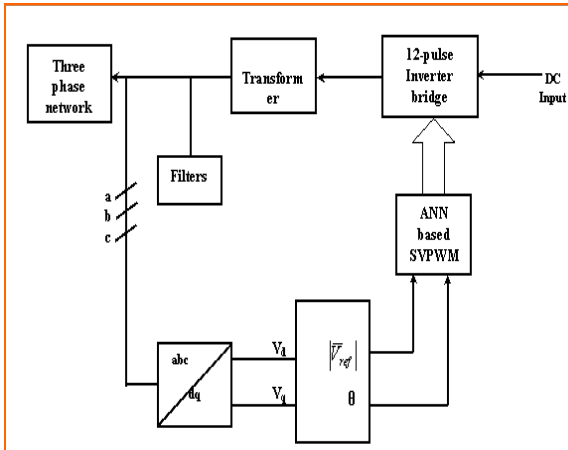


Fig.15: Block diagram represents SVPWM based on ANN with Inverter bridge.

The THD ratio of the line current for switching frequencies 1050Hz and 1450Hz after applying NN is shown in figure. 16.

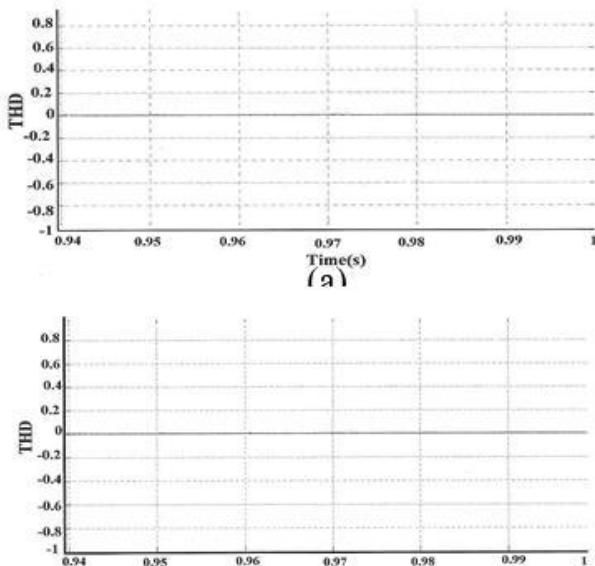


Fig.16: THD ratio of line current in time domain after applying NN based SVPWM.  
 (a) at switching frequency (1050Hz).  
 (b) at switching frequency (1450Hz).

The THD ratio of the line to line voltage for 1050Hz and 1450Hz switching frequencies after applying NN is shown in figure. 17.

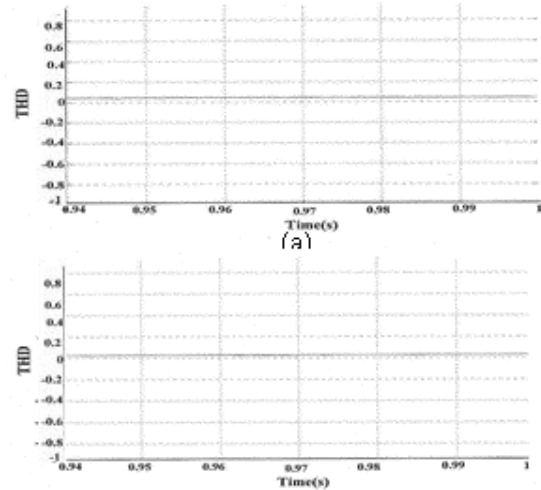


Fig.17: THD ratio of line to line voltage in time domain after applying NN based SVPWM.  
 (a) at switching frequency (1050Hz).  
 (b) at switching frequency (1450Hz).

## IX. CONCLUSION

When using the NN controller based SVPWM the THD value of line current and line to line voltage is improved as a percentage ratio by 74.65% and 78.28% respectively as compared with SVPWM at switching frequency 1050Hz, and these value are improved as a percentage ratio by 68.1% and 65.72% respectively as compared with SVPWM and switching frequency 1450Hz.

At switching frequency 1450Hz the THD ratio is reduced as compared with the switching frequency 1050Hz but the filter losses are increased.

## REFERENCES

- [1] Vijay, K. Sood "HVDC and FACTS Controllers" Kluwer power electronics and power editions series, 2004.
- [2] Michael, P., Johnson, B., and B " the ABC of HVDC Transmission Technologies" , power and energy magazine, 5, March/Aplil 2007.
- [3] Padiyar, K.R., Prabhu, N., " Modeling Control Design and Analysis of VSC Based HVDC Transmission" Paper published in POWERCOM 2004, 21-24 November, Singapore.
- [4] Guangkai, Li., et al " Research on Dynamic Characteristics of VSC-HVDC System " power Engineering Society General Meeting , IEEE, 2006.
- [5] Song, R., et al. " VSCs Based HVDC and its Control Strategy" Electric Power Research Institute, Beijing, China, IEEE/PES Transmission and Distribution Conference 2005.
- [6] Vironis, T. D., et al " Optimal Integration Fan Offshore Wind Farm to a Weak AC Grid" IEEE Transactions on Power delivery , 21,2, April 2006.

- [7] Subrata, K.,Joao,O.P.,Bimal, K.,"A Neural-Network-Based Space-Vector PWM Controller for a Three-Level Voltage-Fed Inverter Induction Motor Drive" *IEEE Transactions on Industry Applications*, 38,3,PP:660-669, 2002.
- [8] Vassilios, G.,A., Georgios, D., D., Nikolas, F., "Recent Advances in High-Voltage Direct-Current Power Transmission Systems",
- [9] Van, H. W., Skudelny, H.C., Stank, G., " Analysis and Realization of a Pulse Width Modulator Based on Voltage Space Vectors" *IEEE Transactions Industry Applications Application*, 24, 1,pp:1530-1535, 1998.
- [10] Bakhshai,A., Joos, G., Esinoza, J., "Fst Space Vector Moulation Based on a Neurocomuting Digital Signal Processor", in *Proc. APEC'97*,pp: 872-878, 1997.
- [11] Amitava D., Debasish L and Barnali K" Space Vector PWM Based AC Output Voltage Control of Z- Source Inverter" *IEEE Transactions on Industry Applications*, January 2, 2010.
- [12] "Pulse-WidthModulation(PWM)Technique"www2.ece.ohio-state.edu/ems/PowerConverter/lect25.ppt
- [13] Abdul Hamid B. and PramodA."An Artificial-Neural – Network- Based Space Vector PWM of a Three-Phase High Power Factor Converter for Power Quality Improvement" *IEEE Transactions on Industry Applications*, January 2, 2010.
- [14]L. Fausett, "Fundamental of Neural Networks, Architectures, Algorithms and applications", Printice Hall Int. Snc., 1994.